Geochemistry, Geophysics, Geosystems®

AGU ADVANCING EARTH AND SPACE SCIENCE

RESEARCH ARTICLE
10.1029/2022GC010685

A >200 ka U-Th Based Chronology From Lacustrine Evaporites, Searles Lake, CA

Justin S. Stroup[1,2], Kristian J. Olson[3], Tim K. Lowenstein[3], Adam B. Jost[2], Hayley M. Mosher[1], Mark D. Peaple[4], Sarah J. Feakins[4], Christine Y. Chen[5], Steven P. Lund[4], and David McGee[2]

[1]Department of Atmospheric and Geological Sciences, State University of New York at Oswego, Oswego, NY, USA, [2]Department of Earth, Atmospheric and Planetary Sciences, Massachusetts Institute of Technology, Cambridge, MA, USA, [3]Department of Geological Sciences and Environmental Studies, State University of New York, Binghamton, NY, USA, [4]Department of Earth Sciences, University of Southern California, Los Angeles, CA, USA, [5]Cosmochemical and Isotopic Signatures Group, Nuclear and Chemical Sciences Division, Lawrence Livermore National Laboratory, Livermore, CA, USA

Key Points:

- >200 ka-long sediment record of southwestern North American paleoenvironment
- Establishes general criteria for selection of evaporite minerals for U-Th dating
- Explores a wide range of parameters for Bayesian age-depth modeling

Supporting Information:

Supporting Information may be found in the online version of this article.

Correspondence to:

J. S. Stroup,
justin.stroup@oswego.edu

Citation:

Stroup, J. S., Olson, K. J., Lowenstein, T. K., Jost, A. B., Mosher, H. M., Peaple, M. D., et al. (2023). A >200 ka U-Th based chronology from lacustrine evaporites, Searles Lake, CA. *Geochemistry, Geophysics, Geosystems*, *24*, e2022GC010685. https://doi.org/10.1029/2022GC010685

Received 1 SEP 2022
Accepted 24 FEB 2023

Author Contributions:

Conceptualization: Justin S. Stroup, Kristian J. Olson, Tim K. Lowenstein, Adam B. Jost, Mark D. Peaple, Sarah J. Feakins, Steven P. Lund, David McGee
Data curation: Justin S. Stroup, Kristian J. Olson, Adam B. Jost, Hayley M. Mosher, David McGee
Funding acquisition: Justin S. Stroup, Tim K. Lowenstein, Sarah J. Feakins, Steven P. Lund, David McGee
Investigation: Justin S. Stroup, Kristian J. Olson, Tim K. Lowenstein, Adam B. Jost, Hayley M. Mosher, Mark D. Peaple, David McGee

Abstract Well-dated lacustrine records are essential to establish the timing and drivers of regional hydroclimate change. Searles Basin, California, records the depositional history of a fluctuating saline-alkaline lake in the terminal basin of the Owens River system draining the eastern Sierra Nevada. Here, we establish a U-Th chronology for the ~76-m-long SLAPP-SLRS17 core collected in 2017 based on dating of evaporite minerals. Ninety-eight dated samples comprising nine different minerals were evaluated based on stratigraphic, mineralogic, textural, chemical, and reproducibility criteria. After the application of these criteria, a total of 37 dated samples remained as constraints for the age model. A lack of dateable minerals between 145 and 110 ka left the age model unconstrained over the penultimate glacial termination (Termination II). We thus established a tie point between plant wax δD values in the core and a nearby speleothem $\delta^{18}O$ record at the beginning of the Last Interglacial. We construct a Bayesian age model allowing stratigraphy to inform sedimentation rate inflections. We find that the >210 ka SLAPP-SRLS17 record contains five major units that correspond with prior work. The new dating is broadly consistent with previous efforts but provides more precise age estimates and enables a detailed evaluation of evaporite depositional history. We also offer a substantial revision of the age of the Bottom Mud-Mixed Layer contact, shifting it from ~130 ka to 178 ± 3 ka. The new U-Th chronology documents the timing of mud and salt layers and lays the foundation for climate reconstructions.

Plain Language Summary Searles Lake, California, is currently a dry saltpan; however, in the past, it was a large and deep lake (>200 m). Lake levels have varied with changes in climate. These changes influenced the sediments deposited. Thus, changes in the lake sediments can be applied to understand the past environments of the region. Here, we developed a chronology for a 76-m-long sediment core using isotopic dating methods. The lake sediments contain many different minerals which can be dated. However, some of these minerals formed after the lake sediments were deposited and others have been chemically altered in the time since their formation. We developed criteria for the selection of samples that are the most likely to reflect the age of sediment deposition. We used the selected ages along with statistical modeling to determine the ages of the sediments with depth. We find that the core contains a record that spans over 200,000 years, including the last two glacial cycles. The age model presented here lays the foundation for the exploration of how past climate changes impacted water availability and vegetation in southeastern California.

1. Introduction

Southwestern North America experienced pronounced changes in precipitation and water availability during Late Pleistocene glacial-interglacial cycles. A diverse array of paleoclimate archives, including lake deposits, speleothems, and packrat middens, document how lake levels, water tables, vegetation, and precipitation patterns have varied (e.g., Bader, 2000; Heusser et al., 2015; Lachniet et al., 2014; Litwin et al., 1999; Lowenstein et al., 1999; Moseley et al., 2016; Oster et al., 2014; Reheis et al., 2014; Thompson & Anderson, 2000; Wendt et al., 2018; Woolfenden, 2003). These archives provide benchmarks that can be used to test how well climate models represent the response of regional hydroclimate to a range of forcings and boundary conditions (e.g., Lora et al., 2017; McGee et al., 2018; Oster et al., 2015; Tabor et al., 2021).

The sedimentary record of the Searles Basin (southeastern California) is a particularly important target for further development (Figure 1). The basin has been the terminus of the Owens River system for much of the last several

Methodology: Justin S. Stroup, Kristian J. Olson, Tim K. Lowenstein, Adam B. Jost, Mark D. Peaple, Sarah J. Feakins, Christine Y. Chen, Steven P. Lund, David McGee
Project Administration: Justin S. Stroup, Tim K. Lowenstein, Sarah J. Feakins, David McGee
Resources: Justin S. Stroup, Tim K. Lowenstein, Sarah J. Feakins, David McGee
Software: Justin S. Stroup, Mark D. Peaple
Supervision: Justin S. Stroup, Tim K. Lowenstein, Sarah J. Feakins, David McGee
Validation: Justin S. Stroup, Kristian J. Olson, Adam B. Jost, David McGee
Visualization: Justin S. Stroup, Kristian J. Olson
Writing – original draft: Justin S. Stroup, Kristian J. Olson, Tim K. Lowenstein, Mark D. Peaple, Sarah J. Feakins, David McGee
Writing – review & editing: Justin S. Stroup, Kristian J. Olson, Tim K. Lowenstein, Adam B. Jost, Hayley M. Mosher, Mark D. Peaple, Sarah J. Feakins, Christine Y. Chen, Steven P. Lund, David McGee

hundred thousand years (Smith, 1979). Since the Owens River is a leading source of water for the Los Angeles metropolitan area, data from the Searles Basin are important for documenting how the water balance of a societally important watershed has responded to past climate changes.

Previous work demonstrated that Searles Basin deposits record dramatic changes in water balance. Lake shoreline deposits range up to ∼200 m above the presently dry basin floor, and sediments from the last glacial period preserve millennial-scale oscillations between salt and mud (Lin et al., 1998; Peng et al., 1978; Phillips et al., 1994; Smith, 1979, 2009). In addition, the basin contains a long sediment record, reaching back to the late Pliocene (3.3 Ma) (Liddicoat et al., 1980). Studies of the more recent Late Pleistocene sediments lay the foundation for explorations of the region's more ancient paleoclimate.

Previous work also presents a conundrum that motivates further development of the Late Pleistocene record from the Searles Basin. During the last glacial period, lake levels in basins across the southwestern U.S., including the Searles and Owens basins, appear to have been high, prior to drying after ∼15 ka during the last deglaciation (Bacon et al., 2006, 2020; Benson et al., 1990; Munroe & Laabs, 2013; Reheis et al., 2014; Rosenthal et al., 2017). Data from nearby Death Valley suggest a similar pattern during previous glacial periods, with higher lake and water table levels during the penultimate glacial period and drying during Termination II (∼130 ka) (Ku et al., 1998; Lowenstein et al., 1999; Wendt et al., 2018). In contrast, Searles Basin sediments have been interpreted to indicate lake deepening rather than drying during Termination II, with deep lakes during the last interglacial period (Bischoff et al., 1985; Smith, 1984). Although this inconsistency has been noted for over 30 years, it remains undetermined whether it results from chronological problems, errors in sedimentological interpretation, or actual climatic or hydrological differences.

Establishing chronologies in evaporite lacustrine environments can be particularly challenging because of sedimentological, mineralogical, and technical considerations. In these environments, sediments are especially susceptible to diagenetic interactions, which must be understood to interpret the timing of sediment deposition and to select syndepositional material for dating. Prior chronologic work (Bischoff et al., 1985; Lin et al., 1998; Peng et al., 1978; Phillips et al., 1983, 1994; Smith, 2009) assumed that the materials dated were syndepositional. In many cases, these studies were also technologically limited by U-Th methods (alpha decay counting in earlier studies, and analysis by thermal ionization mass spectrometry in later studies), which required larger sample sizes (0.5 g to >10 g) that integrated different minerals. Thus, samples were dated without detailed petrographic study. Researchers recognized spurious ages (e.g., Smith, 2009) and identified inconsistencies in existing chronologies (e.g., Knott et al., 2019). While each study advanced the understanding of the region and provided additional layers of chronological information, none established a robust framework for interpreting syndepositional minerals for dating. Olson and Lowenstein (2021) provided a framework for understanding the complexities of sedimentation and diagenesis within the Searles Basin. This work, along with technological advancements that allow the dating of small samples, highlights a need to reassess prior work and provides a foundation for the present study.

This study seeks to enable deeper exploration of the Searles Basin sediment record through the development of an age model for two sediment cores collected near the center of the basin in 2017. We combine U-Th dating of lake precipitates with interpretations of the depositional and diagenetic history of dated samples to obtain robust depositional ages. Using Bayesian age modeling, we apply these ages and one tie point based on a comparison of SLAPP-SRLS17 plant wax hydrogen isotope (δD_{wax}) data (Peaple et al., 2022) and the "Leviathan" speleothem $\delta^{18}O$ record (Lachniet, 2016) to establish an age-depth relationship that serves as the foundation for proxy records from the core. We anticipate that this work will renew the investigation of the basin's response during the penultimate glacial period, Termination II, and the last interglacial, as well as the application of proxies that were not available during previous coring of the basin (e.g., organic biomarkers; Peaple et al., 2022).

2. Stratigraphy and Previous Dating

The subsurface stratigraphy of Searles Lake is characterized by interbedded muds and salts which record hydrologic variability (Figure 1; e.g., Smith, 1979; Smith et al., 1983). Muds were deposited during relatively wet periods and salts formed during dry periods (net evaporation > net inflow). The Lower Salt is subdivided into seven salt layers and six mud layers, and the Mixed Layer is subdivided into nine units, A–I (Figure 1).

Previous work used radiocarbon and U-Th dating to provide age estimates for the uppermost ∼250 ka of Searles Basin sedimentation. All radiocarbon ages from previous work have been recalibrated using INTCAL20 (Reimer

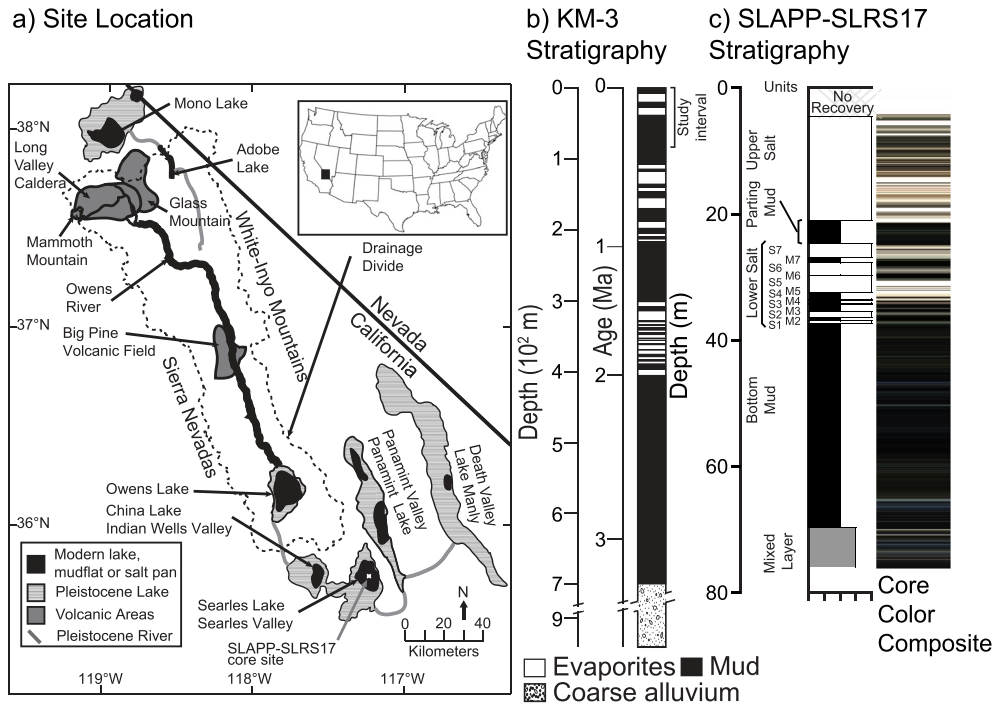

Figure 1. (a) The Searles Basin is located in the Owens River drainage in the southern Sierra Nevada mountain range (California, USA). It is the third basin in a chain of five basins that spilled into one another at times in the past. (b) The KM-3 core (~10 m away from SLAPP-SLRS17) stratigraphy demonstrates that the Searles Basin contains a long sediment record, ~700 m spanning the last ~3.3 Ma. The general stratigraphy has been extensively documented (e.g., Liddicoat et al., 1980; Smith, 1979). (c) SLAPP-SLRS17 stratigraphic column; the units recovered from the bottom up are Mixed Layer, Bottom Mud, Lower Salt (containing alternating salt units S1–S7 and mud units M2–M7), Parting Mud and Upper Salt. The core color composite highlights many small-scale stratigraphic changes not represented in the general stratigraphy. Light colors are evaporite-dominated sediments and darker colors indicate muds; note in many cases, the mud contains abundant evaporite minerals.

et al., 2020), and all U-Th ages have been recalculated using updated decay constants (Cheng et al., 2013) and an initial atomic $^{230}Th/^{232}Th$ ratio of $9 \pm 4 \times 10^{-6}$ (see below for an explanation of this initial value).

Dates from the surface through the Upper Salt span from 3.8 ± 0.3 ka (calibrated ^{14}C date on a wood fragment; Smith, 1979) to 8.8 ± 2.5 ka (U-Th date on salt; Peng et al., 1978), placing this unit within the Holocene. Radiocarbon dating using decay counting of disseminated organic matter in the Parting Mud indicated a basal age of 27 ka and a top age of 12.3 ka (Smith, 1979), roughly corresponding to the Last Glacial Maximum and deglaciation. We consider these dates from disseminated organic matter as estimates due to the potential for modern carbon contamination during the extraction of organic matter to bias ages younger, and the potential for lake reservoir effects and inputs of preaged organic carbon to bias ages older.

Previous U-Th dating of the Lower Salt unit indicated that this interval spans ~35 to 23 ka (Lin et al., 1998; Peng et al., 1978; Phillips et al., 1994). Though the dates have substantial uncertainties and there are some disagreements between U-Th datasets (Text S1 and Figure S1 in Supporting Information S1), the existing U-Th data from the Lower Salt suggest that the basal age of the Parting Mud is ~23 ka, not 27 ka. Phillips et al. (1994) and Lin et al. (1998) suggested that the seven salt units in the Lower Salt correspond to millennial-scale warming events recorded in Greenland ice cores (Interstadials 2–8). Lin et al. (1998) carefully evaluated the initial $^{230}Th/^{232}Th$ ratio for Searles Basin salts, finding that a value of 9×10^{-6} (corresponding to an activity ratio of 1.8) is required to preserve stratigraphic order in U-Th ages from the Lower Salt unit.

Bischoff et al. (1985) used U-Th dating of gaylussite, dolomite, and trona to extend the age model through the Bottom Mud and uppermost Mixed Layer. Their data placed the Bottom Mud-Mixed Layer contact at around 130 ka, near the time of Termination II, and suggested that the Mixed Layer extends beyond 250 ka. Smith (2009) reexamined these ages along with the ^{36}Cl-based age estimates of Jannik et al. (1991) and suggested that the basal age for the Bottom Mud was closer to ~150 ka.

Table 1
List of Common Minerals in the SLAPP-SLRS17 Sediments and Characterization of Qualities Relevant to Interpretations of U-Th Ages

		Environment				Timing			Texture			
				Subsurface						Permeability		Sedimentological assessment of U/Th ages
Mineral	Formula	Water column	Lake floor	Shallow	Deep	Primary	Syndepositional	Burial	Non-porous	High	Low	
1 Halite	$NaCl$		X			X			X			Reliable
2 Aragonite	$CaCO_3$	X				X					X	Reliable
3 Gaylussite	$Na_2Ca(CO_3)_2 \cdot 5H_2O$			X			X		X			Reliable
4 Pirssonite	$Na_2Ca(CO_3)_2 \cdot 2H_2O$			X			X		X			Reliable
5 Trona	$Na_3H(CO_3)_2 \cdot 2H_2O$	X				X	?	?		X		Unreliable
6 Nahcolite	$NaHCO_3$	X				X	?	?		X		Unreliable
7 Burkeite	$Na_6(CO_3)(SO_4)_2$	X				X	?	?	X			Unreliable
8 Borax	$Na_2(B_4O_5)(OH)_4 \cdot 8H_2O$	X		?	X	X	?	?	X			Unreliable
9 Hanksite	$Na_{22}K(SO_4)_9(CO_3)_2Cl$			?	X		?	?	X			Unreliable
10 Aphthitalite	$(K,Na)_3Na(SO_4)_2$	X				X			X			Not Dated
11 Calcite	$CaCO_3$	X				X					X	Not Dated
12 Dolomite	$CaMg(CO_3)_2$	X		X		X	X				X	Not Dated
13 Northupite	$Na_3Mg(CO_3)_2Cl$			X			X		X			Not Dated
14 Thenardite	Na_2SO_4		X			X	X	?	X			Not Dated

Note. Numbered minerals correspond with the numbered minerals in Figures S4–S8 of Supporting Information S1.

Together, existing data from the Searles Basin suggest much lower sedimentation rates of muds than salts. Sedimentation rates in the Upper Salt approach 1 m/ka, whereas rates in the Parting Mud and Bottom Mud are approximately 0.2–0.3 m/ka. However, large uncertainties remain in the age-depth relationship due to low precision of individual ages, substantial scatter in Bottom Mud and upper Mixed Layer ages (Figure S1 in Supporting Information S1), and a lack of detailed characterization of the minerals being dated.

3. Evaporite Minerals in the Searles Basin

The development of an age model for the SLAPP-SRLS17 core requires an understanding of the timing and mechanisms of mineral formation (Figure S2 in Supporting Information S1). The chemical sediments of core SLAPP-SRLS17 are composed of 14 major minerals (carbonates, sulfates, borates, silicates, and chlorides), each of which exhibits a variety of depositional and postdepositional textures (Table 1; Figures S3–S8 in Supporting Information S1). Identifying textures indicative of postdepositional alteration is crucial to using saline minerals for geochronologic analysis.

Olson and Lowenstein (2021) used Pitzer-based thermodynamic models to reproduce the mineral phases, sequences, and abundances observed in core SLAPP-SRLS17 as a function of (a) evaporative concentration of Owens River inflow water, (b) temperature, (c) salinity, (d) pCO_2, and (e) thermodynamic system behavior (*open* or *closed*). Core and thin section textures and fabrics were used to distinguish between primary (cumulate and bottom-growth) and secondary (replacement, cement) minerals. Geochemical and sedimentological analyses were then integrated for each mineral to interpret the environment of deposition (water column, lake floor, shallow subsurface, or deep subsurface), timing of formation (primary, syndepositional, or burial), and chemical processes involved (direct crystallization or back-reaction).

The geochemical modeling and core observations by Olson and Lowenstein (2021) establish a general depositional model for Searles Lake evaporite minerals (Figure S3 in Supporting Information S1). First, alkaline earth carbonates calcite/aragonite [$CaCO_3$] and dolomite [$CaMg(CO_3)_2$] precipitate in the water column and are deposited on the lake floor as massive or laminated chemical muds (Figure 2-I; Figure S4 in Supporting Information S1). As lake level falls and salinity increases, saline-alkaline brines diffuse along density gradients into the

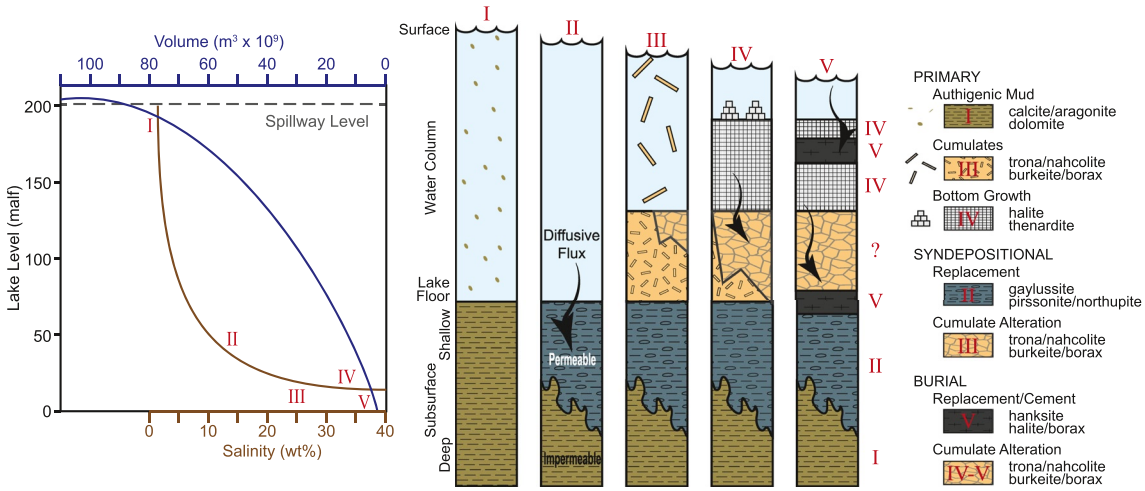

Figure 2. Schematic of mineral formation histories. (left) Lake volume (blue) and salinity (brown) relationships with corresponding facies (I–V). (right) Facies and depositional history diagram. (I) Large lake conditions result in lower salinities and authigenic mud deposition; (II) smaller lake conditions cause increased salinities, creating a density gradient between lake water and pore fluid that drives displacive crystal growth in existing sediments; (III, IV, and V) further reductions in lake volume increase salinity initiating evaporite precipitation and further cementation. Arrows indicate density-driven infiltration of pore fluids by more saline lake bottom water.

underlying lake sediment. The resulting increase in porewater salinity drives in situ, *closed* system back-reactions, with gaylussite [$Na_2Ca(CO_3)_2 \cdot 5H_2O$] replacing calcite/aragonite and northupite [$Na_3Mg(CO_3)_2Cl$] replacing dolomite (Figure 2-II; Figure S4 in Supporting Information S1). Continued diffusion of higher salinity brines drives a reaction with gaylussite to produce pirssonite [$Na_2Ca(CO_3)_2 \cdot 2H_2O$]. The diffusion of ions into sediment pore fluids is limited to the shallow subsurface (Spencer et al., 1985), suggesting that gaylussite, northupite, and pirssonite likely form syndepositionally (Olson & Lowenstein, 2021).

As evaporation continues, Searles Lake brine reaches salt saturation, and trona, nahcolite, burkeite, and borax precipitate within the water column and settle onto the lake floor as cumulates (Figure 2-III; Figure S5 in Supporting Information S1). As Searles Lake brines reach their maximum concentration, halite [NaCl] and thenardite [$NaSO_4$] precipitate directly on the lake floor as bottom-growth (Figure 2-IV; Figure S6 in Supporting Information S1). Void-filling cements are the last to form (Figure 2-V). Hanksite [$Na_{22}K(SO_4)_9(CO_3)_2Cl$] is the predominant void-filling cement and can form by multiple back-reactions depending on the available precursor salts (Olson & Lowenstein, 2021). Hanksite is found at cumulate/mud boundaries and near dense halite layers, suggesting hanksite forms where dense, downward moving brines encounter low permeability layers (Figure S7 in Supporting Information S1). Large volumes of hanksite cement suggest precompaction formation, but the precise timing is unclear.

The depositional model above focuses on how and when each mineral formed from the evolving Searles Lake surface brine. Post-depositional processes also influenced salt preservation in the subsurface of Searles Lake. Cumulates which precipitate seasonally may back-react on the lake floor to equilibrate at bottom water temperatures (Figure 2-III). Cumulate alteration may also occur during early diagenesis due to changes in pore-water chemistry (Figure 2-IV) or during late diagenesis as deposits equilibrate to burial temperatures (Figure 2-V). Thus, while the models of Olson and Lowenstein (2021) establish a framework for interpreting the formation of each mineral, additional work is required to characterize postdepositional processes before the radiometric age of each mineral is interpreted. Here, additional sedimentological analysis is applied to core SLAPP-SRLS17 to identify textures indicative of diagenesis and establish criteria for evaluating the reliability of Searles Lake minerals for U-Th geochronology.

4. Methods

4.1. Core Collection and Description

The Searles Lake Paleoclimate Project (SLAPP) collected two cores using sonic drilling in 2017. The first, SLAPP-SRLS17-1A (35.73715°N, −117.33029°W), extended to 76.7 m below the surface (mbs), and the second

(SLAPP-SRLS17-1B, 35.73715°N, −117.33033°W) extended from 21.7 to 38.8 mbs to provide continuous coverage of millennial-scale salt-mud oscillations in the Lower Salt. Core description, sampling, scanning and photography were completed at the Continental Scientific Drilling (CSD) Facility (formerly the National Lacustrine Core Facility) at the University of Minnesota, Twin Cities, in 2017 (Figure 1c). Gray scale data were extracted from core images using ImageJ. The images were collected directly after core splitting to minimize oxidation. All images were collected with a constant exposure. The data were also used to assemble core color composites. These data are intended to represent the more detailed stratigraphy of the core record not captured by the major stratigraphic units. The SLAPP-SRLS17 cores preserve stratigraphy recognized from previous work in the basin (Smith, 1979, 2009; Smith et al., 1983) from bottom to top including the uppermost Mixed Layer, Bottom Mud, Lower Salt, Parting Mud, and Upper Salt units (Figure 1). The stratigraphy of SLAPP-SRLS17 closely corresponds to the core KM-3, ∼10 m away (Smith et al., 1983).

4.2. Sample Selection and Preparation

Of the 14 major/minor SLAPP minerals, five were excluded from dating (Table 1). Calcite and dolomite were excluded due to sample impurities (low U/Th ratios) as well as uncertainties regarding detrital versus authigenic and primary versus diagenetic origins. Northupite crystals could not be cleanly separated from the muddy matrix due to their small, submillimeter size. Aphthitalite [$(K, Na)_3Na(SO_4)_2$] is typically found encased in hanksite cement, from which it could not be cleanly separated. Bottom-growth thenardite was found in a single layer, but initial screening (Section 4.3) revealed U/Th atomic ratios of ∼1, too low for U/Th analysis. Dating attempts were made on the remaining nine minerals (Table 1).

Once a dating horizon and mineral were identified, crystals were handpicked and precleaned to remove detrital material. The evaporite crystals were covered in sediment (mud, other mineral grains), which was removed by rinsing, sonicating, and mixing repeatedly by vortexing in pure ethanol to clean the exterior of the crystals. The samples were scrubbed and rinsed with a small paint brush and ethanol squirt bottle until the exteriors of the crystals were clean of loose debris.

We then evaluated the crystals under a binocular microscope. Crystals with many sediment inclusions were rejected. The exteriors of sediment-free crystals or solid crystal masses were scraped and/or cleaved to separate the interior for dating. This cleaning process reduced debris that was stuck on crystal surfaces and removed exterior surfaces that may have recrystallized (producing younger ages) or lost uranium (causing ages to appear older). Each crystal was then cleaved into smaller portions and inspected for additional inclusions, signs of secondary crystallization (smaller infilling crystals), or fluid penetration (cracks). Clean crystal fragments were collected until enough material was gathered for U-Th screening and dating.

Sample materials were identified by XRD and visual inspection. Sample mineralogies are indicated in the data archived at the NOAA paleoclimatology database (Stroup et al., 2022). XRD was performed on most samples used for dating. We did not perform XRD on the exact material dated for samples 44, 51, 71, and 73 (listed as halite & borax) and samples 24, 45, 48, 49, and 74 (listed as halite & trona); for these samples, XRD was done on the bulk material prior to cleaning and picking samples. These samples, however, are thought to be pure halite; if they contained trace amounts of trona or borax, they would still be considered minimum depositional ages.

4.3. U-Th Analysis

We screened most samples for their ^{238}U and ^{232}Th concentrations to identify samples with relatively low detrital contamination and to estimate the amount of material and spike required for high-precision U-Th analyses. For screening, we isolated ∼1 mg subsamples and dissolved them in 1.5 mL of 0.5 M nitric acid. If undissolved solids were observed after 1 hr of reaction time, we used a pipette to remove ∼1 mL of the solution and left behind the solids. We then introduced samples into a quadrupole ICP-MS (Agilent 7900) at MIT and measured ^{43}Ca, ^{232}Th, and ^{238}U. A standard containing Ca, U, and Th was analyzed at varying concentrations to establish a linear calibration between signal intensity and concentration, and the standard was analyzed after every ∼15–20 samples to track calibration changes during the analytical session. Samples with atomic $^{238}U/^{232}Th$ ratios >10 were prioritized for U-Th dating, but we also dated samples with lower U/Th ratios in high-priority intervals. This screening allowed us to focus analyses on samples with low detrital contamination.

In addition, screening was important for determining sample weights necessary to achieve appropriate U contents (∼10–100 ng) for U-Th dating, as U concentrations ranged from ∼5 ng/g to 346 μg/g in our samples—almost

five orders of magnitude. Due to this large range of concentrations, samples for dating ranged in mass from 0.2 to 593 mg (the average sample mass was 10 mg, and the median was 25 mg). We note that the small sample sizes used in this study represent an important advance over previous U-Th dating of Searles Basin deposits, as they allowed us to target particularly clean and/or dense material. Sample sizes in previous studies ranged from 0.5 g for TIMS-based analyses (Lin et al., 1998) to 10 g or more for decay-counting methods (Bischoff et al., 1985; Peng et al., 1978).

Samples selected for U-Th dating were processed using standard procedures in a clean laboratory at MIT (Text S2 in Supporting Information S1). Measured U and Th isotope ratios were corrected for background, tailing, mass bias, ion counter yield, contributions of naturally occurring isotopes in the tracer, and procedural blank. Ages were determined using the ^{238}U half-life of Jaffey et al. (1971) and the ^{234}U and ^{230}Th half-lives of Cheng et al. (2013). Ages were corrected for contributions from initial ^{230}Th using the ^{230}Th/^{232}Th ratio determined by Lin et al. (1998) from analyses of the Lower Salt (9×10^{-6} atomic). We assigned a 95% confidence interval of 4×10^{-6} to account for temporal variations in this ratio.

4.4. Age Model Development

We used the Bayesian modeling package Bacon (Blaauw & Christen, 2011; Trachsel & Telford, 2017) for the age-depth model construction because the multiple mud-salt transitions in the Searles cores necessitated a model that can incorporate changing model parameters with stratigraphic position. We used Bacon Version 2.5.7, which can accommodate extreme changes in sedimentation rates and multiple stratigraphic units. Since model priors can be challenging to set (Trachsel & Telford, 2017), we took an iterative approach to determine the various parameters applied to generate age models. We ran more than 40 different combinations of model configurations to assess model parameter selection and the impacts of our selection criteria (Supporting Information S1). We compared model results against the U-Th age data, stratigraphy, and other model runs. We varied the initial parameters until the resulting age model was no longer consistent with data or diverged. We compared the age model against the U-Th ages and rejected parameter sets that caused the model to bypass viable ages, exhibit bias and/or react too stiffly to unit changes. In cases of divergence, we found that some combinations of parameters caused the model to completely depart from the data. Based on these tests, we chose the parameters that yielded solutions consistent with age and stratigraphic data, and we evaluated a series of additional cross-parameter interactions and sensitivities.

The final model was constructed using the boundaries of each stratigraphic unit (Upper Salt, Parting Mud, Lower Salt, Bottom Mud, Mixed Layer). It was particularly important to select model sections (segments) that (a) matched unit thicknesses in the core; (b) used a small value for memory to accommodate large changes in sedimentation regimes between evaporite and mud deposition; and (c) included appropriate initial accumulation rates for each unit. Age modeling parameters are described in Text S3 in Supporting Information S1. Several dating samples were from the same or nearby stratigraphic locations but not from the same material. Thus, we treat them as individual ages in the Bacon model inputs. All ages are plotted individually in Figure 3.

5. Results

5.1. Evaporite Textures

Gaylussite and pirssonite occur as microscopic to cm-scale crystals in mud units. Crystals commonly contain noncalcareous inclusions. In laminated units, gaylussite crystals grow along and/or cross-cut laminations (Figure S4 in Supporting Information S1); a variety of growth fabrics occur in thin-bedded and massive units. Crystal textures varied among units but were typically uniform within a single depositional unit. However, in some instances, multiple populations of crystals were identified in a single unit by differing crystal morphology, orientation, or size.

Cumulates are defined as fine, well sorted, euhedral crystals which precipitate at the surface (rafts) or within the water column and then settle onto the lake floor. Layers with trona, nahcolite, halite, thenardite, aphthitalite, and borax meet these criteria. Cumulate layers are deposited with high primary porosity and are thus highly permeable except where cemented (see Figures S4–S8 in Supporting Information S1 for more textural and mineralogical information). Trona and nahcolite display a variety of additional textures, including blades, splays, and

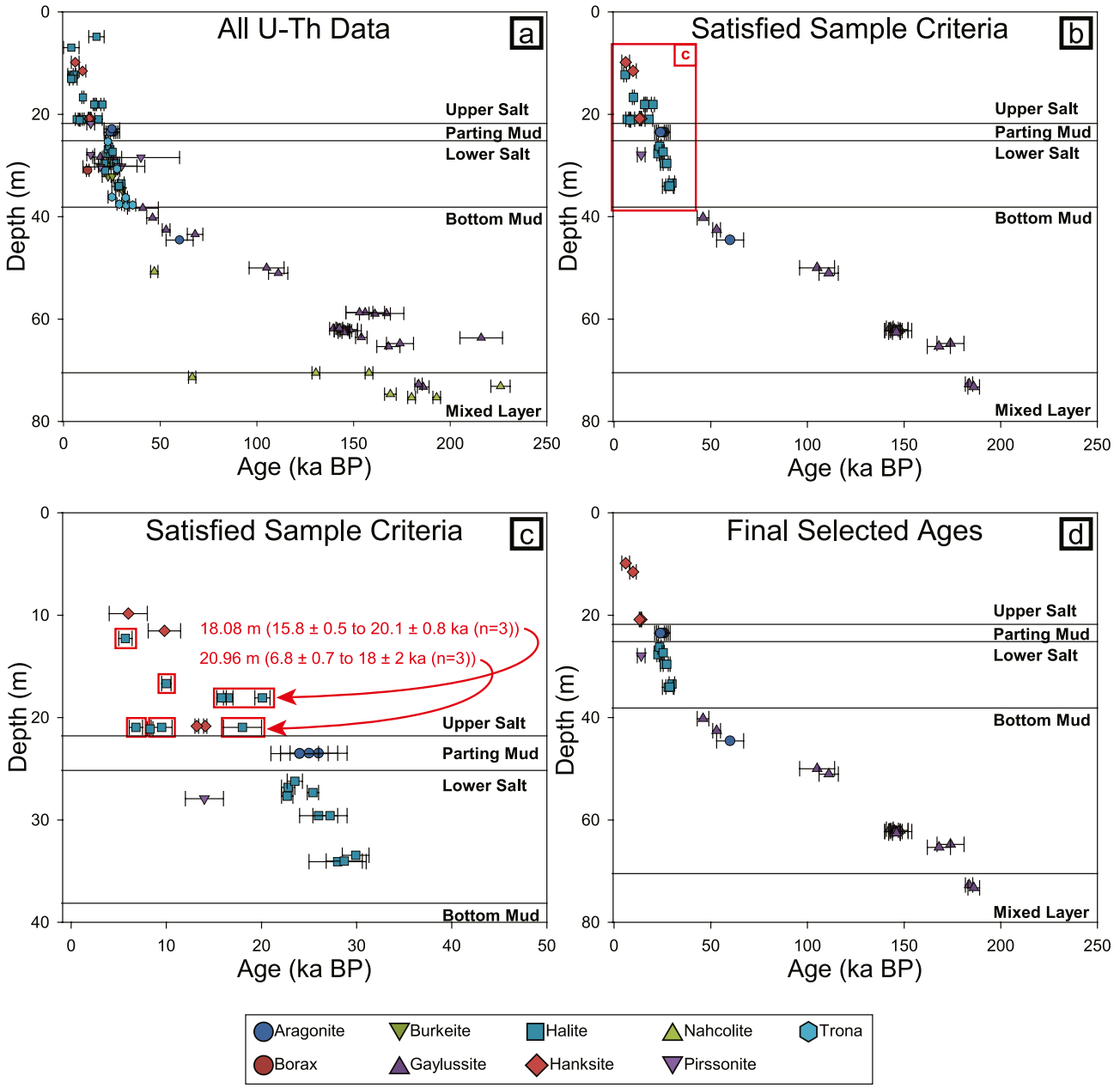

Figure 3. U-Th dating results. (a) All U-Th results. Ninety-eight (98) samples from 9 mineral categories were dated. (b) Forty-six ages passed the sedimentological and U-Th criteria. Retained ages in the Mixed Layer, Bottom Mud, and Lower Salt are internally consistent and reproducible. Halite ages in the Upper Salt (red box in c) show inconsistencies. (c) Upper Salt ages, showing rejected halite ages and retained hanksite ages, minimum depositional ages (see main text). (d) Thirty-seven ages were used for age modeling.

overgrowths. Burkeite displays variable features but lacks unambiguous cumulate textures. Generally, burkeite occurs as large vuggy masses composed of microcrystalline mosaics with abundant inclusions, typically trona cumulates. Burkeite can also be found as crystalline mosaics of interstitial material, some of which may be cement.

The textural criteria for recognizing halite bottom-growth are well established (Hardie et al., 1985; Lowenstein & Hardie, 1985). Bottom growth halite forms mm-scale crystals free of mud inclusions, typically associated with finely crystalline trona cumulates (Figure S6 in Supporting Information S1). In some cases, alteration of interstitial material results in dissolution and rounding of halite grain boundaries (Figure S8 in Supporting Information S1).

Pore-filling cements include hanksite, borax, and halite. Cements are typically free of mud inclusions. Hanksite and borax are also found in mud units. In these instances, borax occurs as large single crystals free of inclusions.

In contrast, large hanksite crystals in mud units contain abundant included salts—typically cumulates of trona, thenardite, aphthitalite, borax, and halite.

5.2. U-Th Ages

We determined a total of 98 U-Th ages on samples from SLAPP-SLRS17 cores (data archived at the NOAA paleoclimatology database; Figure 3a). These ages include 23 replicates (samples of the same mineralogy and core depth). Samples included halite, gaylussite, nahcolite, trona, and aragonite, and ages ranged from 3.9 to 280 ka. The data set suggests a general age-depth relationship that is broadly consistent with previous findings (e.g., Bischoff et al., 1985) (Supporting Information S1), but several ages were not in stratigraphic order. To determine which U-Th results to include in the age model, we developed criteria to prioritize syndepositional minerals over post- or diagenetic minerals and identify ages least likely to have experienced open-system behavior with respect to U.

6. Discussion

6.1. Age Evaluation

We developed and applied sedimentological and U-Th criteria to identify appropriate samples for chronology. We also considered the influences of past mining operations on the sediments to determine a selection of ages appropriate for age modeling.

6.1.1. Sedimentological Criteria for Age Selection

The sedimentological criteria for age selection are based on the timing of mineral formation and suitability of minerals for U-Th geochemistry (Table 1). Additional sedimentological analysis is applied here to identify textures indicative of (a) postdepositional alteration and (b) possible *open* system behavior (i.e., uranium loss), both of which may impart age biases. Primary textures and low porosity are important considerations when selecting samples for U-Th dating because porous sediments with high hydraulic conductivity may allow leaching of soluble uranium from crystal boundaries, resulting in artificially older ages (Prado-Pérez et al., 2013). In the following paragraphs, we describe features (macroscopic and in thin section) that were used to determine which samples to include in the final age-depth model.

Early replacement minerals include gaylussite/pirssonite, which is formed from reactions between sediment and pore fluids. Density-driven diffusion of ions from lake brine into the pore space of underlying sediment is predicted to occur during periods when Searles Lake level fell and salinity increased. Such brine infiltration and pore water salinity increase led to replacement of calcite/aragonite by gaylussite, and later gaylussite replacement by pirssonite (Olson & Lowenstein, 2021). Ion diffusion models for the Great Salt Lake show that the diffusive flux below a halite bed can extend to ~2 m below the sediment-water interface (Spencer et al., 1985). For Searles Lake, however, the uptake of ions during gaylussite formation limits the diffusive depth of Na^{2+} and CO_3^{2-}. Gaylussite-bearing units overlain and underlain by unaltered calcite/aragonite (Figure S4a in Supporting Information S1) indicate that the diffusion front forming gaylussite may be limited to ~10 cm below the sediment-water interface. The formation of pirssonite from gaylussite is similarly limited in scale (Figure S3 in Supporting Information S1). Gaylussite and pirssonite are therefore interpreted to form syndepositionally, near the sediment-water interface, and are appropriate for U-Th dating. Nonetheless, later diagenetic processes may produce gaylussite and pirssonite which requires additional examination to determine burial diagenetic textures and fabrics.

Gaylussite crystal size, abundance, and growth fabric are controlled by the amount and distribution of aragonite and calcite in the mud layers. Gaylussite textures are therefore expected to vary from layer to layer but should be uniform within individual layers. On the other hand, layers with multiple populations of gaylussite indicate several episodes of diagenetic crystal growth (Figure S4 in Supporting Information S1). Such units were excluded from age modeling. Although late diagenetic gaylussite is predicted to yield a younger age than the surrounding sediment, these minerals instead yielded ages that biased old (Figures 3a and 3d). This observation suggests that subsurface brines interacted with and removed soluble uranium from gaylussite crystals, which produced older than true ages.

Most cumulate layers from the SLAPP-SLRS17 cores display textures indicative of diagenetic alteration (dissolution, overgrowth, replacement, recrystallization; Text S4 in Supporting Information S1). Alteration of cumulates

may occur syndepositionally due to seasonal brine temperature variations (Figure 2-III) or after deposition as salts equilibrate with burial temperatures (Figure 2-V). Alteration may be enhanced by subsurface brine movement. In contrast to fine-grained muds with low permeability, the flow of brines through cumulate layers may be substantial because layers composed of randomly oriented crystals have exceedingly high porosity (Figure S4 in Supporting Information S1). Detailed sedimentological analysis of cumulates is therefore required to determine the criteria that can be used to identify the timing and mechanisms of diagenetic alteration.

Many of the Searles Lake cumulates have been altered by dissolution, overgrowth, recrystallization, or replacement. The complex textures (Figures S5 and S8 in Supporting Information S1) make it difficult to discern the timing of diagenesis. Cumulates with alteration textures are therefore excluded from age model consideration. In addition, the high porosity of all cumulates makes such layers susceptible to open system uranium loss (Figure S5 in Supporting Information S1). Cumulates are therefore excluded from age model considerations, with the notable exception of aragonite laminae, which occur in relatively impermeable mud units.

Primary bottom growth halite contains mud-free, mm-sized single crystals. Bottom growth halite is therefore a good target for U–Th dating, although low U concentrations can make precise dating difficult. Bottom growth halite is typically codeposited with cumulates (Figure S6 in Supporting Information S1). In some cases, alteration of associated cumulate crystals produced dissolution and rounding of halite grain boundaries (Figure S8 in Supporting Information S1). Crystal boundaries are easily avoided during sampling (see Section 4.2).

Cements composed of hanksite are mud free and therefore ideal for U-Th dating. However, it is not possible to distinguish the precise timing of cement formation (Hardie et al., 1985). Hanksite cements fill porous uncompacted crystalline frameworks suggesting early, possibly syndepositional, precipitation (Figure S7 in Supporting Information S1). Despite the uncertain timing of formation, hanksite ages nonetheless provide the most internally consistent and reproducible ages in the Upper Salt. These ages are retained in the age model, as explained in more detail in Section 6.1.4.

6.1.2. U-Th Criteria for Age Selection

We applied two additional criteria aimed at identifying samples that were minimally affected by detrital contamination and thus most likely to have remained closed systems with respect to U and Th, following the approach of Chen et al. (2020).

First, we identified low-detritus samples by removing all samples with $^{230}Th/^{232}Th$ atomic ratios less than 36×10^{-6}. As the initial $^{230}Th/^{232}Th$ ratio is estimated to be $9 \pm 4 \times 10^{-6}$ in the Searles Basin (Lin et al., 1998), our criterion is equivalent to 4 times the estimated initial value. While the precise value of this criterion is subjective, it is intended to identify samples that are the most sensitive to corrections for initial ^{230}Th, producing imprecise age estimates and raising questions about the accuracy of corrected ages. In total, 18 samples were removed due to this criterion, including 16 that passed mineralogical selection criteria.

To identify samples that were most likely to have remained closed systems with respect to U and Th, we defined a final criterion using the initial $\delta^{234}U$ value calculated for the authigenic portion of each sample. $\delta^{234}U$ is expressed in units of per mil (‰) and is defined as follows:

$$\delta^{234}U = (([^{234}U/^{238}U) - 1) * 1000 \quad (1)$$

where $(^{234}U/^{238}U)$ is an activity ratio. A sample at secular equilibrium has $(^{234}U/^{238}U)$ of 1 and a $\delta^{234}U$ value of 0. "Initial" $\delta^{234}U$, or $\delta^{234}U_0$, is the $\delta^{234}U$ corrected for decay of ^{234}U since the formation of the mineral:

$$\delta^{234}U_0 = \delta^{234}U * e^{\lambda 234 * t} \quad (2)$$

where λ_{234} is the decay constant for ^{234}U (Cheng et al., 2013), and t is the age of the mineral.

We then corrected $\delta^{234}U_0$ values for detrital U. We identified the fraction of detrital U using the measured $^{238}U/^{232}Th$ ratios and a detrital $^{238}U/^{232}Th$ ratio of 0.25 ± 0.10 (the ratio corresponding to a detrital $^{230}Th/^{232}Th$ ratio of $9 \pm 4 \times 10^{-6}$ and detrital matter with ^{230}Th and ^{238}U in secular equilibrium) (Chen et al., 2020). We assumed a $\delta^{234}U$ value of 0 for detrital U and determined the initial $\delta^{234}U$ values necessary for nondetrital (authigenic) U to produce the initial $\delta^{234}U$ values determined for the bulk sample. We refer to these estimates of the initial $\delta^{234}U$ values of authigenic precipitates as $\delta^{234}U_{0,auth}$.

Unusually high values for $\delta^{234}U_{0,auth}$ indicate samples with anomalously old ages due to U loss, as the age correction will "overcorrect" measured $\delta^{234}U$ values for age decay. In order to use this criterion, however, we must first determine a reasonable range for $\delta^{234}U_{0,auth}$ values in Searles Basin precipitates.

Most natural waters have positive $\delta^{234}U$ values due to preferential leaching of ^{234}U from radiation-damaged sites and mineral surfaces (Chabaux et al., 2003). $\delta^{234}U$ values in rivers and closed-basin lakes vary due to changes in chemical and physical weathering intensity and/or changes in U source (Grzymko et al., 2007; McGee, 2012; Robinson et al., 2004). In the Searles Basin, $\delta^{234}U_{0,auth}$ values appear to have varied within a narrow range over the last 30 ka despite dramatic changes in temperature and precipitation accompanying the last glacial termination. $\delta^{234}U_{0,auth}$ values of samples that met the sedimentological criteria from the Lower Salt, Parting Mud and Upper Salt range from 191 to 281‰. We applied this range for the remainder of the SLAPP-SRLS17 sediments. We excluded samples with $\delta^{234}U_{0,auth} > 290$‰, as these samples are likely to have lost uranium, producing anomalously old ages. We identified five samples with $\delta^{234}U_{0,auth}$ values greater than 290‰, which includes 3 samples that passed all other criteria.

6.1.3. Evaluation of Retained Ages

Forty-six (46) ages were retained based on the sedimentological and U-Th criteria described above. The ages consisted primarily of halite in the Upper Salt and Lower Salt, aragonite in the Parting Mud, and gaylussite in the Bottom Mud and Mixed Layer (Figure S3 in Supporting Information S1). Ages from these samples are stratigraphically consistent, with limited exceptions discussed below (Figure 3b). The resulting age-depth data set is also broadly consistent with previous dating of Searles Basin sediments but with substantially reduced uncertainties (see Section 6.2.3) (Figure S1 in Supporting Information S1).

Importantly, gaylussite ages in the uppermost Bottom Mud (35–43 m) are consistent with nearby ages from primary salts (aragonite, halite), suggesting that gaylussite formed syndepositionally (within the precision of the age model) (Figures 3a and 3d). This observation lends confidence to our reliance on ages from gaylussite in the lowermost 30 m of the core. The single pirssonite age is anomalously young (Figure 3b), suggesting that replacement of gaylussite by pirssonite may occur well after sediment deposition.

Here, we focus on two remaining problems with dating samples. First, there is a wide range of ages in the Upper Salt, discussed in Section 6.1.4. Second, no ages were obtained between 51.03 and 61.79 m due to a lack of samples that passed mineralogical and U-Th criteria. In Section 6.2.1, we refine the age model in this interval, which contains Termination II.

6.1.4. Upper Salt Ages and the Impact of Solution Mining

The ages of halite crystals in the Upper Salt included scatter beyond calculated measurement uncertainties (Figures 3b and 3c). For example, at 18.08 m, ages range from 15.8 ± 0.5 to 20.1 ± 0.8 ka ($n = 3$), and at 20.96 m, ages range from 6.8 ± 0.7 to 18 ± 2 ka ($n = 3$). We hypothesize that this lack of reproducibility reflects past mining operations in the Upper Salt. Mining operations prior to the 1970s involved extracting brine from Searles Basin salt units. During the 1970s, extraction methods changed, and hot unprocessed brines were reinjected into the Upper Salt to encourage dissolution and generate higher borax yields. Brine was injected into the base of the Lower and Upper Salts under the assumption that the hot brine would rise through the salt. Brine flow therefore may have produced the dissolution and reprecipitation of evaporite minerals, and in particular halite, the most soluble salt in Searles Basin deposits. While the precise locations of brine pumping are not known to the authors, the core site is near the center of the basin, an area of current and past solution mining, and is likely to have been affected by the brine injection.

Partial dissolution of halite is likely to remove uranium and leave behind thorium, a process that would produce dates older than the true depositional age. Secondary precipitation of salts along crystal boundaries and in voids and fractures may also impact Upper Salt deposits; if included in dated samples, these secondary precipitates would bias dates to be younger than their depositional age. Even with the removal of the outer surface of each sample and visual inspection for secondary minerals and cracks during sample preparation, it is likely that Upper Salt halite samples incorporated secondary materials due to small fractures and voids within crystals. As we cannot determine a priori which dates from Upper Salt halite samples are accurate, we reject all Upper Salt halite ages from the age model. We speculate that the divergence of ages observed here is also the reason that only one U-Th age has previously been reported from the Upper Salt (Peng et al., 1978).

To provide age constraints for the Upper Salt, we used hanksite ages. Hanksite forms large euhedral crystals less susceptible to dissolution and reprecipitation than smaller, more soluble halite and trona crystals with larger surface areas. Two hanksite samples from the same stratigraphic interval at 20.83 m gave similar ages (13.2 ± 0.2 and 14.1 ± 0.17 ka). While these ages do not agree within uncertainty, this difference plausibly reflects the duration of hanksite formation during diagenesis. These ages, therefore, should be considered minimum ages, which suggests that the transition from the Parting Mud to the Upper Salt occurred at or before 14.1 ka. Assuming that high lake levels existed during mud deposition and that salt deposits reflect lower lake levels, Searles Lake level fell and disconnected from Owens and China Lake at or before 14.1 ka.

Shoreline data from China Lake support this conclusion. Rosenthal et al. (2017) demonstrated that China Lake and Searles Lake were interconnected between 17 and 14 ka. Radiocarbon dating of gastropod and mollusk shells in the China Lake Basin and uppermost Searles Basin (Salt Wells Valley) suggests diminished connection and declining lake levels in the Searles basin beginning at 14.1 ka. This age agrees with the oldest hanksite age from the Upper Salt and suggests that hanksite precipitation occurred shortly after the onset of lake level drawdown and Upper Salt deposition. While there may have been a brief rise of China Lake at ∼13.2 ka, by 13–12.6 ka gastropods that inhabited spring discharge aprons indicate falling lake levels and exposure of groundwater seeps in the China Basin (Rosenthal et al., 2017).

We noted above that solution mining also took place in the Lower Salt, raising the question of why it did not produce similar effects on evaporite minerals in this unit. We hypothesize that mining had relatively less effect on Lower Salt ages due to the interlayered muds (Figure 1), which would have limited fluid flow between salt units.

6.2. Age Model

Combining the various rejection criteria and mining history, we retained 37 U-Th ages to establish a chronology for the SLAPP-SLRS17 core. We constructed an age model with the Bayesian age-depth modeling program Bacon (Blaauw & Christen, 2011; Supporting Information S1; Figure S9 in Supporting Information S1). We evaluated age-depth relationships using stratigraphic information and a proxy comparison.

6.2.1. Age Model Refinement and Tie Point Establishment

We note two gaps in the age model (44.55–49.98 m and 51.03–61.79 m) that result in a lack of robust age constraints between 55–100 ka and 110–145 ka (Figure 3d and Figure S9 in Supporting Information S1). The lower gap contains Termination II, the penultimate glacial termination. Previous work and our dating of SLAPP-SRLS17 demonstrate that Termination I (the most recent glacial termination) was accompanied by marked changes in lake level and sedimentation rates in the Searles Basin (Lin et al., 1998; Phillips et al., 1994; Smith, 1979). Given the evidence from southeastern California sites for basin desiccation and lowering of groundwater tables across both Termination I and II (Lowenstein et al., 1999; Szabo et al., 1994; Wendt et al., 2018), there is reason to suspect that Termination II was also marked by changes in lake level and sedimentation rate in Searles Basin. However, without radiometric ages, the U-Th-based age model projects a linear sedimentation rate throughout the 110–145 ka interval (Figure 3 and Figure S9 in Supporting Information S1).

Plant wax hydrogen isotope (δD_{wax}) measurements from SLAPP-SRLS17 sediments provide a means of refining the age model across Termination II. The SLAPP-SLRS17 C_{31} *n*-alkane δD record (hereafter SLAPP δD_{wax}) is published (Peaple et al., 2022). δD_{wax} values primarily track changes in precipitation δD values (Feakins & Sessions, 2010; Sachse et al., 2012). Similarly, regional speleothem $\delta^{18}O$ values are thought to primarily reflect changes in precipitation $\delta^{18}O$ values (Lachniet et al., 2014; Moseley et al., 2016). Assuming minimal lag in the recording of precipitation $\delta^{18}O$ and δD values by speleothems and sedimentary plant waxes, respectively, we expect good agreement between δD_{wax} and speleothem $\delta^{18}O$. During the last 100 ka, there is generally good correspondence (within age model uncertainty) between SLAPP δD_{wax} and $\delta^{18}O$ changes recorded in the Devils Hole and Leviathan records (see the Supporting Information S1 for evaluation of offsets; Lachniet et al., 2014; Moseley et al., 2016) with more positive values during warm periods (MIS5e, 5c and 5a, as well as MIS3 and MIS1) and more negative values during the MIS4 and MIS2 glacial periods, as well as during MIS5d and MIS5b (Figure 4 and Figure S10 in Supporting Information S1). Below, we assess this agreement more quantitatively.

In contrast, we observe a clear discrepancy between SLAPP δD_{wax} and regional speleothem $\delta^{18}O$ records during Termination II (Figure 4a). While speleothem records show a steep rise in $\delta^{18}O$ values during Termination II

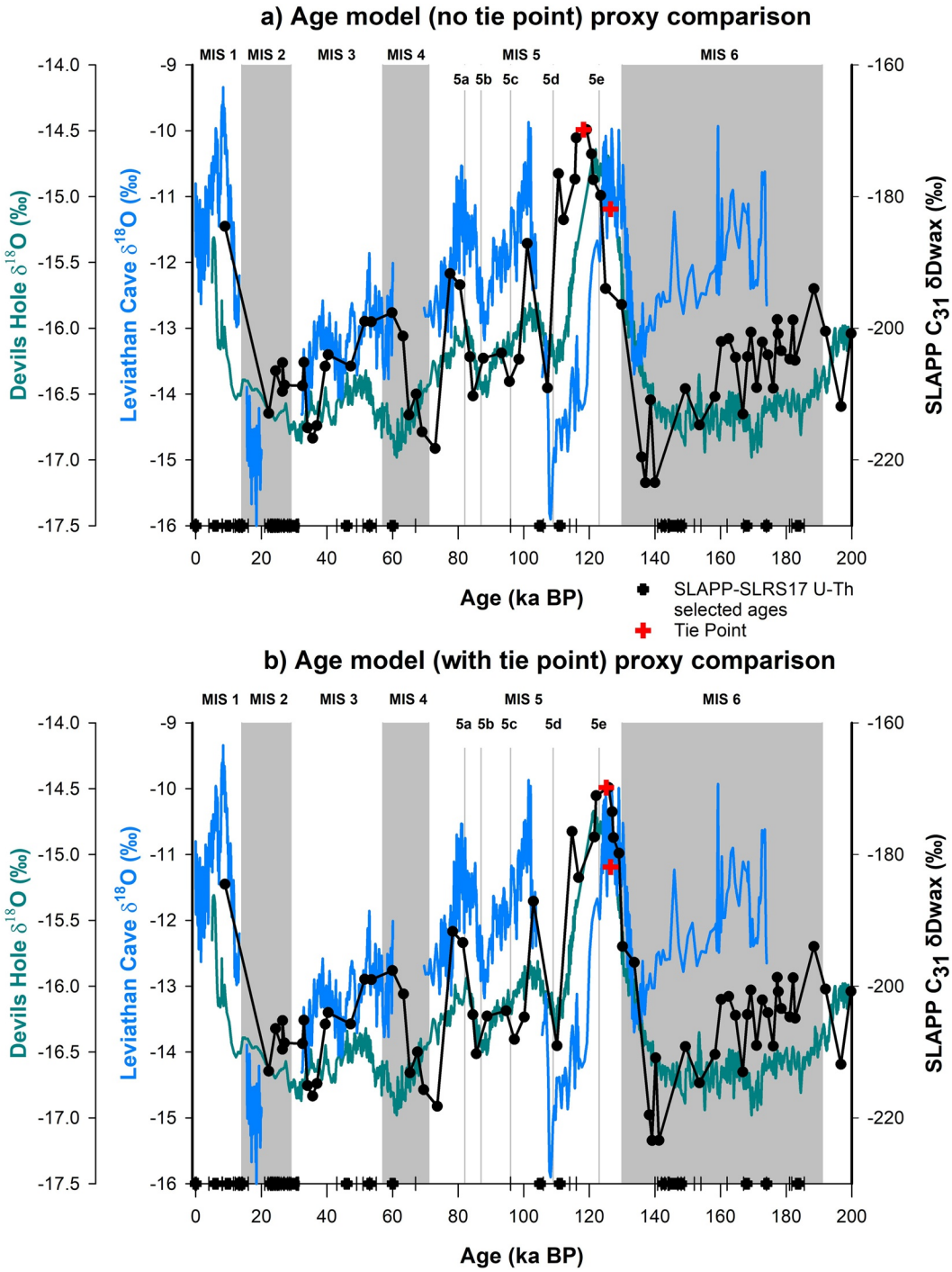

Figure 4. Evaluation of age model performance using comparison of SLAPP-SLRS17 C_{31} *n*-alkane δD record (Peaple et al., 2022), the Leviathan $\delta^{18}O$ compilation from Leviathan, Lehman, and Pinnacle Caves (Lachniet, 2016) and Devils Hole $\delta^{18}O$ (Moseley et al., 2016). MIS stages (gray bars) indicated (Lisiecki & Raymo, 2005). (a) There is good agreement over the last 100 ka, but an offset of ~8 ka exists at Termination II. This likely results from changing sedimentation rates which are unconstrained by a lack of U-Th ages between 110 and 145 ka in the SLAPP-SLRS17 record. We establish a tie point with the Leviathan $\delta^{18}O$ record (red cross) and apply it to produce a final age model (Figure 5). (b) Comparison of Leviathan and Devils Hole $\delta^{18}O$ with SLAPP-SLRS17 δD_{wax} data using the age model with the tie point. Note that because Bacon does not force the age model to pass directly through the tie point, the mean age of the tie point in the SLAPP-SRLS17 age model is slightly offset from the age of the tie point in the Leviathan record.

and high values during MIS5e, an increase in SLAPP δD_{wax} appears approximately ~8 ka later on the U-Th age model. Based on the agreement in regional $\delta^{18}O$ records and the SLAPP δD_{wax} record over the last 100 ka, we argue that this mismatch during Termination II reflects imprecision in the SLAPP-SLRS17 age model due to the lack of age constraints around this time.

To address this gap, we introduce a tie point between the Leviathan speleothem $\delta^{18}O$ record (Lachniet et al., 2014) and the SLAPP δD_{wax} record at the peak of MIS5e. We established this tie point by matching the peak nearest to 125 ka in the SLAPP δD_{wax} record to the MIS5e peak in the Leviathan speleothem $\delta^{18}O$ compilation (Figure 4 and Text S5, Figures S10 and S11 in Supporting Information S1). To determine the tie point location, we normalized both records, interpolated them to a constant 0.1 ka timestep, and then applied a low pass Butterworth filter to remove high frequency variability. We then defined tie points where the first derivatives of the interpolated, filtered records reached zero nearest to 125 ka (Supporting Information S1). This indicated an age of 126.5 ka at 54.5 m depth for the SLAPP-SLRS17 record.

We assign an uncertainty of 2 ka (2σ) to the MIS5e tie point. This assigned error is intended to account for similar uncertainties in the temporal correspondence between δD_{wax} changes in the Searles Basin and $\delta^{18}O$ values in regional speleothems across the rest of MIS5 (Figure S11 in Supporting Information S1) as well as age uncertainties in the Leviathan record, which in this section of the record range from 0.2 to 0.9 ka (2σ) (Lachniet, 2016). An additional consideration for the tie point's uncertainty involves the response of Bacon to the inclusion of the tie point in the age model. Bacon consistently directed the age-depth relationship through the young end of the tie point's confidence interval (Figure S12 in Supporting Information S1). This occurs because Bacon's default is to maintain relatively constant sedimentation rates in regions of the model with few age constraints. With a large uncertainty, the tie point approaches the no-tie point age model (Figure S12 in Supporting Information S1). Only when tie point uncertainties were reduced to 2 ka did the tie point constrain the age model such that the mean age offsets at the tie point that were similar in magnitude to the offsets observed for the MIS5a, 5c and 5d extremes (i.e., ~2–3 ka) (Figure S11 in Supporting Information S1). The model returns a mean age of 124.6 ka for the MIS5e SLAPP δD_{wax} peak, which is 2.0 ka after the Leviathan MIS 5e peak (the tie point) and 1.3 ka before the MIS 5e peak in the Devils Hole record (Figure S11 in Supporting Information S1).

We incorporated the tie point age, error, and depth into the Bacon age model (Figure 5 and Text S6 in Supporting Information S1). The introduction of a tie point results in higher sedimentation rates during the end of MIS6 and a reduction in sedimentation rates during the first half of the MIS5. The tie point eliminates our ability to assess leads and lags between the Searles Basin and regional speleothem records during Termination II. However, our analysis of other portions of MIS5 suggests that these leads and lags are within the uncertainty of the SLAPP age model.

We note two remaining portions of the SLAPP δD_{wax} record that appear to show substantial offsets with regional speleothem records: MIS2 and MIS4. In MIS2, the transition to more positive δD_{wax} values appears to begin well before $\delta^{18}O$ values in the Leviathan and Devils Hold records begin to rise. However, this is an artifact of low sampling resolution in this portion of the SLAPP δD_{wax} record. Salts with low organic content occur during Termination I, so no δD_{wax} data exist between ~22 and 9 ka. We are thus unable to constrain the timing of the rise in δD_{wax} values across Termination I. In MIS4, the minimum δD_{wax} values in the SLAPP record occur well before the minimum values in the Devils Hole record (the Leviathan record lacks data in this interval.) As in Termination II, this offset is likely to reflect a change in the sedimentation rate that is not resolved by the U-Th age model, as there are no U-Th data between 55 and 100 ka. We choose not to introduce a second tie point here because it would strongly nudge the model toward the orbital frequencies present in the Devils Hole and/or Leviathan records, reducing our ability to compare orbital variability in the various records (Peaple et al., 2022).

6.2.2. Sedimentation Rates

In the Searles Basin, evaporite depositional rates outpaced those of muds. Rapid deposition of salt is observed in modern basins such as the Dead Sea, where 2 m of halite was deposited within ~40 years as water levels fell ~30 m since 1980 (Lensky et al., 2005; Lowenstein et al., 2021). In Death Valley, California, a 186-m-long core from the center of Badwater Basin had an average sedimentation rate of 1 m/ka. Evaporite minerals (predominantly halite) were deposited much faster (~1.7–3.8 m/ka) and mud deposition was slower (0.4–1 m/ka) (Lowenstein et al., 1999). In the SLAPP-SLRS17 record, average accumulation rates for the units vary similarly (Figure 5): Upper Salt (~1.4 m/ka), Parting Mud (0.5 m/ka), Lower Salt (0.8 m/ka), Bottom Mud (0.2 m/ka), Mixed Layer (0.4 m/ka).

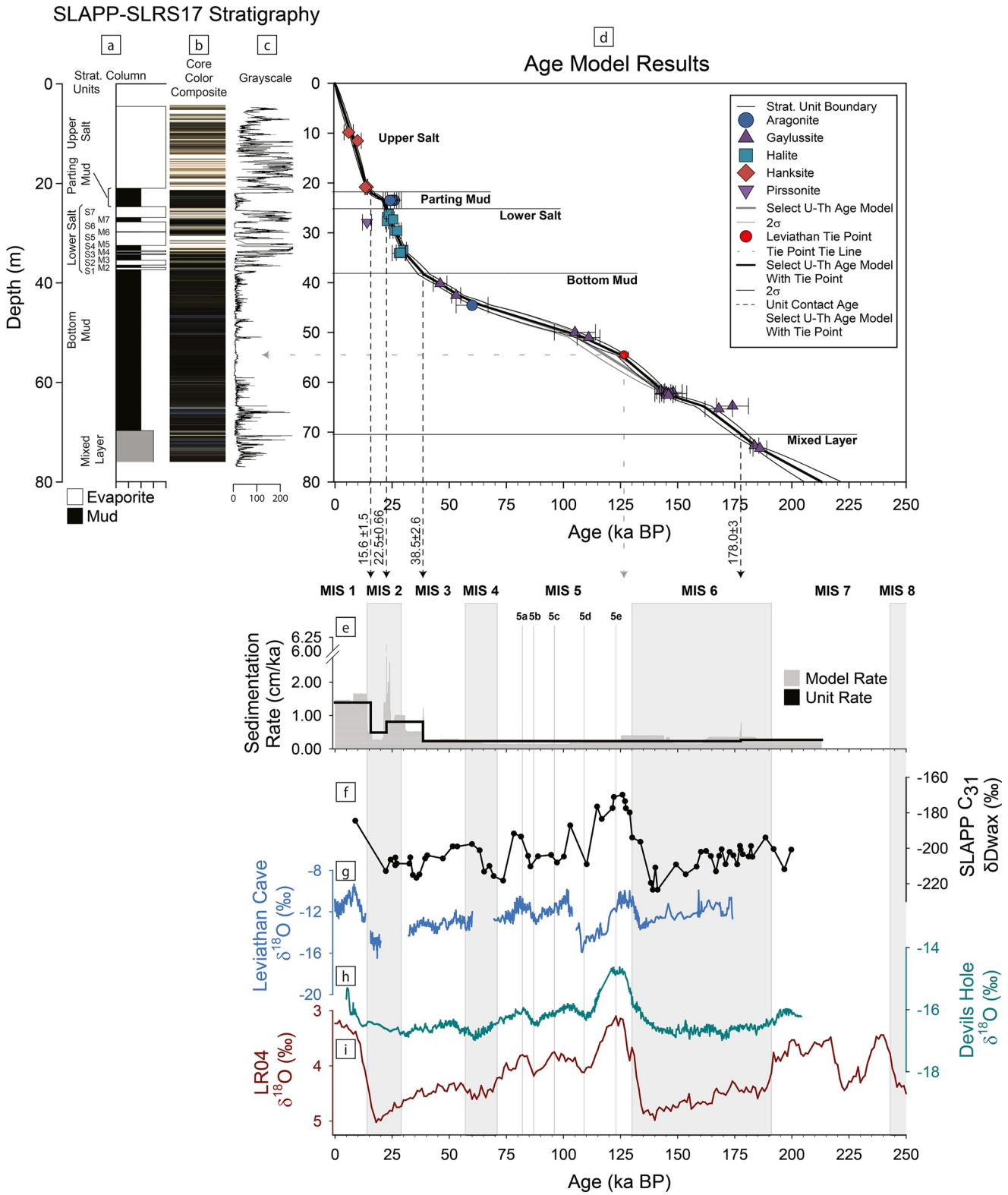

Figure 5. Age-depth relationship for the SLAPP-SLRS17 core. (a) General stratigraphy; (b) core color composite; (c) grayscale profile; (d) final age model (black), using 37 U-Th ages and the tie point, constructed with Bacon using optimized model parameters (see main text and Supporting Information S1). The age model based on only U-Th ages is shown in gray. Model mean and 95% confidence interval shown for both models. (e) Sedimentation rate extracted from the age model (gray) and average sedimentation rate by unit (black). (f) SLAPP-SLRS17 C_{31} *n*-alkane δD record (Peaple et al., 2022); (g) Leviathan composite $\delta^{18}O$ record (Lachniet, 2016), (h) Devils Hole $\delta^{18}O$ record (Moseley et al., 2016), and (i) LR04 benthic $\delta^{18}O$ record (Lisiecki & Raymo, 2005).

We note several limitations in our characterization of sedimentation rates. While the age model indicates a higher sedimentation rate in the Lower Salt compared to the Bottom Mud, the core has many changes in lithology (Figure 1), which may correspond to sedimentation rate changes. The Lower Salt, for example, contains seven alternating salts (S1–S6) and muds (M2-M7) (Figure 1). These subunits range in thickness from ∼18 to 220 cm. Cumulatively, the unit contains approximately 650 cm of salt and 420 cm of mud. Despite our best efforts to isolate minerals, viable samples are generally spaced more widely than the units and are not necessarily located near subunit boundaries. Thus, the sedimentation rate suggested by the age model is represented as an average rate across lithologies, providing a maximum rate of mud deposition and a minimum rate of evaporite deposition.

6.2.3. Comparison With Previous Searles Basin Chronologies

The SLAPP-SRLS17 age model reproduces the broad features of prior dating of Searles Basin sediments (Text S1 and Figure S1 in Supporting Information S1). The Upper Salt broadly spans from the late deglaciation to the late Holocene; the Parting Mud was deposited during the Last Glacial Maximum and early deglaciation; the Lower Salt spans the latter part of MIS3 through the Last Glacial Maximum; and the Bottom Mud extends from MIS3 to the last interglacial (MIS5) and beyond. However, closer comparison shows many significant differences in age and analytical uncertainty. Individual U-Th ages from this study have substantially lower uncertainties than ages from previous work, due to improvements in U-Th geochronology—chiefly the switch from alpha decay counting to measurement by inductively coupled plasma mass spectrometry. Through the careful application of sedimentological and U-Th criteria, we are also able to identify the dates that most closely reflect depositional ages, reducing scatter in the age-depth relationship.

In the Upper Salt, near the Upper Salt-Parting Mud boundary, an age from Peng et al. (1978) is ∼5–6 ka younger than those from the SLAPP-SRLS17 record, perhaps due to inclusion of secondary salts in the large (>10 g) Peng et al. sample. Our data suggest that the transition to the Upper Salt occurred by 14.1 ka, based on the dating of hanksite at the base of the Upper Salt. As noted above, this date is consistent with the last ages of sustained high lake levels recorded in the China Lake Basin, which coalesced with the Searles Basin at high water levels. The combination of these data suggests lake drawdown beginning around 14.1 ka. The SLAPP-SRLS17 age model places the age of the Upper Salt-Parting Mud boundary substantially older at 15.6 ka. This age is biased old, as the lack of age constraints between 13.2 and 24.5 ka leads the age-depth model to project constant sedimentation rates over this interval. More likely, slow sedimentation in the Parting Mud occurred until ∼14.1 ka, followed by rapid accumulation of the Upper Salt.

An additional key new finding is that Termination II occurs in the Bottom Mud rather than at the Bottom Mud/Mixed Layer contact, as suggested by Bischoff et al. (1985). The new age model suggests that the Bottom Mud/Mixed Layer contact instead occurs at 178 ± 3 ka, agreeing within uncertainty with the timing of lake level rise in the Death Valley basin at the beginning of MIS6 (186 ± 17 ka; Lowenstein et al., 1999). Related to this finding, we observe that many of the gaylussite ages from Bischoff et al. (1985) are younger than samples from similar depths in SLAPP-SRLS17. While some of this difference may reflect differences in sedimentation rates between the two core sites, the large samples dated by Bischoff et al. (1985) may have included secondary salts with much younger ages, such as the nahcolite from near the Bottom Mud-Mixed Layer boundary, also dated in this study (Figure 3a). The inclusion of these secondary minerals may have led to ages that appear younger.

6.3. Lessons for Future Work Using U-Th on Lake Precipitates

This study shows that U-Th dating of lacustrine evaporites must take mineralogical and textural information into account, as summarized in Figure S2 of Supporting Information S1. U-Th dates from minerals that form during or very soon after deposition provide useful constraints on sediment ages, whereas later diagenetic minerals only provide minimum ages. In addition, mineral textures and stratigraphic associations (e.g., crystal distribution controlled by surrounding sedimentary layers vs. crystals that crosscut these layers) provide essential information on the reliability of associated U-Th ages. In this study, dating and mineralogical observations were conducted concurrently; it would have been more efficient to conduct mineralogical observations first, and then focus U-Th dating on syndepositional minerals more likely to have exhibited closed system behavior.

U-Th ages of many different minerals and textures can provide information beyond chronology for the sedimentary record. They can be applied to distinguish between primary and secondary textures and demonstrate secondary crystal formation. For example, sedimentological criteria excluded trona from the age model (high

permeability), but ages from trona samples are in close agreement with the model, suggesting the preservation of depositional ages (Figure 3a).

Second, we suggest various quality control tests for identifying the most reliable U-Th ages, applying a similar approach to Chen et al. (2020). Here, we use the $^{230}Th/^{232}Th$ ratio to identify samples with low detrital contamination, and we use the initial $\delta^{234}U$ value of authigenic material along with reproducibility to identify samples that have been likely to have remained closed systems with respect to U and Th.

Third, we note the utility of screening for ^{238}U and ^{232}Th concentrations in all samples prior to U-Th dating. This screening was essential for identifying samples with low detrital content and for determining appropriate sample and spike amounts for dating, given the very wide range of ^{238}U and ^{232}Th concentrations in samples due to varying mineralogy and lake conditions. The time added by screening is a small fraction of the time spent conducting full U-Th sample preparation and analysis on samples with low $^{238}U/^{232}Th$ ratios or samples with overestimated or underestimated ^{238}U contents.

Finally, we argue that tie points may still be necessary in U-Th-based age models for lake sediments (e.g., Rodbell et al., 2022), but that these should be introduced as sparingly as possible and with thoughtful consideration as to what scientific questions are removed from consideration once the age model has been tuned to other time series.

7. Conclusion

The diverse evaporite mineralogy of the Searles Basin enables insights into past lake conditions but poses significant challenges in establishing a robust chronology because of formation from an array of deposition and diagenetic processes. Extensive evaluation and clear criteria must be applied to determine the ages appropriate for dating such sediments. Our U-Th dating of 98 samples covering nine different mineral categories validates interpretations that some groups are primary or syndepositional, while other minerals are secondary (ages younger than depositional ages) or subject to postdepositional U loss (ages older than depositional ages). Our criteria target syndepositional materials with low detrital contamination, uranium isotope data consistent with closed-system behavior, and good reproducibility in a given depth range. We used 37 ages for age model construction using the Bayesian age-depth modeling package Bacon with carefully chosen parameters that account for stratigraphic changes in the core.

We find that the SLAPP-SRLS17 record extends to >200 ka, recording two full glacial-interglacial cycles. We included a tie point during Termination II using δD_{wax} data from the SLAPP-SRLS17 core (126.5 ka at 54.5 m) and the Leviathan speleothem $\delta^{18}O$ record to fill an important chronological gap in the record where no datable material was available. This single tie point reduces the ability to use the record for studies of the precise phasing of events across Termination II but preserves the ability to study orbital signals and glacial-interglacial variability in the data set. The age model lays the foundation for further work using Searles Basin sediments to probe the hydrological and ecological history of the region and provides several lessons learned for future work using U-Th dating to develop high-quality chronologies from evaporite minerals.

Acknowledgments
This study was supported by U.S. National Science Foundation Grant NSF-EAR—1903519, 1903544, 1903659, and 1903665, respectively, to Stroup, McGee, Lowenstein, and Feakins and a Comer Science and Education Foundation Grant to McGee and Lowenstein. We thank Searles Valley Minerals and especially Jade Zimmerman for access, logistical support and local knowledge of the site. We thank Joe Janick for assistance during on-site drilling and initial core description. Support was provided by the CSD Facility, University of Minnesota, during core collection and during the initial core description, especially Ryan O'Grady, Kristina Brady, Mark Shapley, and Anders Noren. We thank Richard Frieman for technical support at SUNY Oswego. Special thanks to Maarten Blaauw for consultations regarding Bacon and its application to this sedimentary environment.

Conflict of Interest

The authors declare no conflicts of interest relevant to this study.

Data Availability Statement

Data files are archived at the NOAA paleoclimatology database (https://doi.org/10.25921/wrk3-tj55; Stroup et al., 2022).

References

Bacon, S. N., Burke, R. M., Pezzopane, S. K., & Jayko, A. S. (2006). Last glacial maximum and Holocene lake levels of Owens Lake, eastern California, USA. *Quaternary Science Reviews*, *25*(11–12), 1264–1282. https://doi.org/10.1016/j.quascirev.2005.10.014

Bacon, S. N., Jayko, A. S., Owen, L. A., Lindvall, S. C., Rhodes, E. J., Schumer, R. A., & Decker, D. L. (2020). A 50,000-year record of lake-level variations and overflow from Owens Lake, eastern California, USA. *Quaternary Science Reviews*, *238*, 106312. https://doi.org/10.1016/j.quascirev.2020.106312

Bader, N. E. (2000). Pollen analysis of Death Valley sediments deposited between 166 and 114 ka. *Palynology*, *24*(1), 49–61. https://doi.org/10.2113/0240049

Benson, L. V., Currey, D. R., Dorn, R. I., Lajoie, K. R., Oviatt, C. G., Robinson, S. W., et al. (1990). Chronology of expansion and contraction of four Great Basin lake systems during the past 35,000 years. *Palaeogeography, Palaeoclimatology, Palaeoecology*, *78*(3–4), 241–286. https://doi.org/10.1016/0031-0182(90)90217-u

Bischoff, J. L., Rosenbauer, R. J., & Smith, G. I. (1985). Uranium-series dating of sediments from Searles Lake: Differences between continental and marine climate records. *Science*, *227*(4691), 1222–1224. https://doi.org/10.1126/science.227.4691.1222

Blaauw, M., & Christen, J. A. (2011). Flexible paleoclimate age-depth models using an autoregressive gamma process. *Bayesian Analysis*, *6*(3), 457–474. https://doi.org/10.1214/11-ba618

Chabaux, F., Riotte, J., & Dequincey, O. (2003). U-Th-Ra fractionation during weathering and river transport. *Reviews in Mineralogy and Geochemistry*, *52*(1), 533–576. https://doi.org/10.2113/0520533

Chen, C. Y., McGee, D., Woods, A., Pérez, L., Hatfield, R. G., Edwards, R. L., et al. (2020). U-Th dating of lake sediments: Lessons from the 700 ka sediment record of Lake Junín, Peru. *Quaternary Science Reviews*, *244*, 106422. https://doi.org/10.1016/j.quascirev.2020.106422

Cheng, H., Edwards, R. L., Shen, C.-C., Polyak, V. J., Asmerom, Y., Woodhead, J., et al. (2013). Improvements in ^{230}Th dating, ^{230}Th and ^{234}U half-life values, and U–Th isotopic measurements by multi-collector inductively coupled plasma mass spectrometry. *Earth and Planetary Science Letters*, *371*, 82–91. https://doi.org/10.1016/j.epsl.2013.04.006

Feakins, S. J., & Sessions, A. L. (2010). Controls on the D/H ratios of plant leaf waxes in an arid ecosystem. *Geochimica et Cosmochimica Acta*, *74*(7), 2128–2141. https://doi.org/10.1016/j.gca.2010.01.016

Grzymko, T. J., Marcantonio, F., McKee, B. A., & Stewart, C. M. (2007). Temporal variability of uranium concentrations and ^{234}U/^{238}U activity ratios in the Mississippi river and its tributaries. *Chemical Geology*, *243*(3–4), 344–356. https://doi.org/10.1016/j.chemgeo.2007.05.024

Hardie, L. A., Lowenstein, T. K., & Spencer, R. J. (1985). The problem of distinguishing between primary and secondary features in evaporites. In *Paper presented at 6th International Symposium on Salt 1985* (Vol. 1, pp. 11–39).

Heusser, L. E., Kirby, M. E., & Nichols, J. E. (2015). Pollen-based evidence of extreme drought during the last Glacial (32.6–9.0 ka) in coastal southern California. *Quaternary Science Reviews*, *126*, 242–253. https://doi.org/10.1016/j.quascirev.2015.08.029

Jaffey, A., Flynn, K., Glendenin, L., Bentley, W. t., & Essling, A. (1971). Precision measurement of half-lives and specific activities of ^{235}U and ^{238}U. *Physical Review C*, *4*(5), 1889–1906. https://doi.org/10.1103/physrevc.4.1889

Jannik, N. O., Phillips, F. M., Smith, G. I., & Elmore, D. (1991). A ^{36}Cl chronology of lacustrine sedimentation in the Pleistocene Owens River system. *Geological Society of America Bulletin*, *103*(9), 1146–1159. https://doi.org/10.1130/0016-7606(1991)103<1146:accols>2.3.co;2

Knott, J. R., Liddicoat, J. C., Coe, R. S., & Negrini, R. M. (2019). Radiocarbon and paleomagnetic chronology of the Searles Lake Formation, San Bernardino County, California, USA. In *From Saline to Freshwater: The Diversity of Western Lakes in Space and Time*. Geological Society of America Special.

Ku, T.-L., Luo, S., Lowenstein, T. K., Li, J., & Spencer, R. J. (1998). U-series chronology of lacustrine deposits in Death Valley, California. *Quaternary Research*, *50*(3), 261–275. https://doi.org/10.1006/qres.1998.1995

Lachniet, M. S. (2016). A Speleothem Record of Great Basin Paleoclimate: The Leviathan Chronology, Nevada. In *Developments in Earth Surface Processes* (Vol. 20, pp. 551–569). Elsevier.

Lachniet, M. S., Denniston, R. F., Asmerom, Y., & Polyak, V. J. (2014). Orbital control of western North America atmospheric circulation and climate over two glacial cycles. *Nature Communications*, *5*(1), 1–8. https://doi.org/10.1038/ncomms4805

Lensky, N., Dvorkin, Y., Lyakhovsky, V., Gertman, I., & Gavrieli, I. (2005). Water, salt, and energy balances of the Dead Sea. *Water Resources Research*, *41*(12), W12418. https://doi.org/10.1029/2005wr004084

Liddicoat, J. C., Opdyke, N. D., & Smith, G. I. (1980). Palaeomagnetic polarity in a 930-m core from Searles Valley, California. *Nature*, *286*, 22–25.

Lin, J. C., Broecker, W. S., Hemming, S. R., Hajdas, I., Anderson, R. F., Smith, G. I., et al. (1998). A reassessment of U-Th and ^{14}C ages for late-glacial high-frequency hydrological events at Searles Lake, California. *Quaternary Research*, *49*(1), 11–23. https://doi.org/10.1006/qres.1997.1949

Lisiecki, L. E., & Raymo, M. E. (2005). A Pliocene-Pleistocene stack of 57 globally distributed benthic δ^{18}O records. *Paleoceanography*, *20*(1), PA1003. https://doi.org/10.1029/2004pa001071

Litwin, R. J., Smoot, J. P., Durika, N. J., & Smith, G. I. (1999). Calibrating Late Quaternary terrestrial climate signals: Radiometrically dated pollen evidence from the southern Sierra Nevada, USA. *Quaternary Science Reviews*, *18*(10–11), 1151–1171. https://doi.org/10.1016/s0277-3791(98)00111-5

Lora, J. M., Mitchell, J. L., Risi, C., & Tripati, A. E. (2017). North Pacific atmospheric rivers and their influence on western North America at the Last Glacial Maximum. *Geophysical Research Letters*, *44*(2), 1051–1059. https://doi.org/10.1002/2016gl071541

Lowenstein, T. K., & Hardie, L. A. (1985). Criteria for the recognition of salt-pan evaporites. *Sedimentology*, *32*(5), 627–644. https://doi.org/10.1111/j.1365-3091.1985.tb00478.x

Lowenstein, T. K., Li, J., Brown, C., Roberts, S. M., Ku, T.-L., Luo, S., & Yang, W. (1999). 200 ky paleoclimate record from Death Valley salt core. *Geology*, *27*(1), 3–6. https://doi.org/10.1130/0091-7613(1999)027<0003:kyprfd>2.3.co;2

Lowenstein, T. K., Weldeghebriel, M. F., Sirota, I., Eyal, H., Mor, Z., & Lensky, N. G. (2021). Criteria for the recognition of clastic halite: The modern Dead Sea shoreline. *Sedimentology*, *68*(6), 2253–2269. https://doi.org/10.1111/sed.12907

McGee, D. (2012). Absolute-dated, high-resolution records of water balance changes during the last glacial period and deglaciation from lacustrine cave deposits in the Bonneville Basin, Utah, USA. *Quaternary International*, *279*, 317. https://doi.org/10.1016/j.quaint.2012.08.894

McGee, D., Moreno-Chamarro, E., Marshall, J., & Galbraith, E. (2018). Western US lake expansions during Heinrich stadials linked to Pacific Hadley circulation. *Science Advances*, *4*(11), eaav0118. https://doi.org/10.1126/sciadv.aav0118

Moseley, G. E., Edwards, R. L., Wendt, K. A., Cheng, H., Dublyansky, Y., Lu, Y., et al. (2016). Reconciliation of the Devils Hole climate record with orbital forcing. *Science*, *351*(6269), 165–168. https://doi.org/10.1126/science.aad4132

Munroe, J. S., & Laabs, B. J. (2013). Temporal correspondence between pluvial lake highstands in the southwestern US and Heinrich Event 1. *Journal of Quaternary Science*, *28*(1), 49–58. https://doi.org/10.1002/jqs.2586

Olson, K. J., & Lowenstein, T. K. (2021). Searles Lake evaporite sequences: Indicators of late Pleistocene/Holocene lake temperatures, brine evolution, and pCO_2. *Bulletin*, *133*(11–12), 2319–2334. https://doi.org/10.1130/b35857.1

Oster, J. L., Ibarra, D. E., Winnick, M. J., & Maher, K. (2015). Steering of westerly storms over western North America at the Last Glacial Maximum. *Nature Geoscience*, *8*(3), 201–205. https://doi.org/10.1038/ngeo2365

Oster, J. L., Montañez, I. P., Mertz-Kraus, R., Sharp, W. D., Stock, G. M., Spero, H. J., et al. (2014). Millennial-scale variations in western Sierra Nevada precipitation during the last glacial cycle MIS 4/3 transition. *Quaternary Research*, *82*(1), 236–248. https://doi.org/10.1016/j.yqres.2014.04.010

Peaple, M. D., Bhattacharya, T., Lowenstein, T. K., McGee, D., Olson, K. J., Stroup, J. S., et al. (2022). Biomarker and pollen evidence for late Pleistocene pluvials in the Mojave Desert. *Paleoceanography and Paleoclimatology*, *37*(10), e2022PA004471. https://doi.org/10.1029/2022pa004471

Peng, T.-H., Goddard, J., & Broecker, W. (1978). A direct comparison of ^{14}C and ^{230}Th ages at Searles Lake, California. *Quaternary Research*, *9*(3), 319–329. https://doi.org/10.1016/0033-5894(78)90036-4

Phillips, F. M., Campbell, A. R., Smith, G. I., & Bischoff, J. L. (1994). Interstadial climatic cycles: A link between western North America and Greenland? *Geology*, *22*(12), 1115–1118. https://doi.org/10.1130/0091-7613(1994)022<1115:iccalb>2.3.co;2

Phillips, F. M., Smith, G. I., Bentley, H. W., Elmore, D., & Gove, H. E. (1983). Chlorine-36 dating of saline sediments: Preliminary results from Searles Lake, California. *Science*, *222*(4626), 925–927. https://doi.org/10.1126/science.222.4626.925

Prado-Pérez, A., Vázquez, M. C., Vargas, M. J., Sánchez, A. M., & del Villar, L. P. (2013). Sample quality index to preselect suitable carbonate samples for alpha spectrometry U/Th dating. *Applied Radiation and Isotopes*, *73*, 32–43. https://doi.org/10.1016/j.apradiso.2012.11.015

Reheis, M. C., Adams, K. D., Oviatt, C. G., & Bacon, S. N. (2014). Pluvial lakes in the Great Basin of the western United States—A view from the outcrop. *Quaternary Science Reviews*, *97*, 33–57. https://doi.org/10.1016/j.quascirev.2014.04.012

Reimer, P. J., Austin, W. E., Bard, E., Bayliss, A., Blackwell, P. G., Ramsey, C. B., et al. (2020). The IntCal20 Northern Hemisphere radiocarbon age calibration curve (0–55 cal kBP). *Radiocarbon*, *62*(4), 725–757. https://doi.org/10.1017/rdc.2020.41

Robinson, L. F., Henderson, G. M., Hall, L., & Matthews, I. (2004). Climatic control of riverine and seawater uranium-isotope ratios. *Science*, *305*(5685), 851–854. https://doi.org/10.1126/science.1099673

Rodbell, D., Hatfield, R., Abbott, M., Chen, C., Woods, A., Stoner, J., et al. (2022). 700,000 years of tropical Andean glaciation. *Nature*, *607*, (7918), 301–306. https://doi.org/10.1038/s41586-022-04873-0

Rosenthal, J. S., Meyer, J., Palacios-Fest, M. R., Young, D. C., Ugan, A., Byrd, B. F., et al. (2017). Paleohydrology of China Lake basin and the context of early human occupation in the northwestern Mojave Desert, USA. *Quaternary Science Reviews*, *167*, 112–139. https://doi.org/10.1016/j.quascirev.2017.04.023

Sachse, D., Billault, I., Bowen, G. K., Chikaraishi, Y., Dawson, T. E., Feakins, S. J., et al. (2012). Molecular paleohydrology: Interpreting the hydrogen-isotopic composition of lipid biomarkers from photosynthesizing organisms. *Annual Review of Earth and Planetary Sciences*, *40*(1), 221–249. https://doi.org/10.1146/annurev-earth-042711-105535

Smith, G. I. (1979). *Subsurface stratigraphy and geochemistry of late Quaternary evaporites, Searles Lake, California* (Vol. 1043). US Government.

Smith, G. I. (1984). Paleohydrologic regimes in the southwestern Great Basin, 0–3.2 my ago, compared with other long records of "global" climate. *Quaternary Research*, *22*(1), 1–17. https://doi.org/10.1016/0033-5894(84)90002-4

Smith, G. I. (2009). *Late Cenozoic geology and lacustrine history of Searles Valley, Inyo and San Bernardino Counties, California*. US Geological Survey.

Smith, G. I., Barczak, V., Moulton, G. F., & Liddicoat, J. C. (1983). Core KM-3, a surface-to-bedrock record of late Cenozoic sedimentation in Searles Valley, California (pp. 2330–7102). https://doi.org/10.3133/pp1256

Spencer, R., Eugster, H., Jones, B., & Rettig, S. (1985). Geochemistry of Great Salt Lake, Utah I: Hydrochemistry since 1850. *Geochimica et Cosmochimica Acta*, *49*(3), 727–737. https://doi.org/10.1016/0016-7037(85)90167-x

Stroup, J. S., Olson, K., Lowenstein, T. K., Adam, B. J., Mosher, H. M., Peaple, M., et al. (2022). NOAA/WDS Paleoclimatology - Searles Lake California, U-Th chronology and Grayscale Data for SLAPP-SRLS17-1A/B, Late Pleistocene. https://doi.org/10.25921/wrk3-tj55

Szabo, B. J., Kolesar, P. T., Riggs, A. C., Winograd, I. J., & Ludwig, K. R. (1994). Paleoclimatic inferences from a 120,000-yr calcite record of water-table fluctuation in Browns Room of Devils Hole, Nevada. *Quaternary Research*, *41*(1), 59–69. https://doi.org/10.1006/qres.1994.1007

Tabor, C., Lofverstrom, M., Oster, J., Wortham, B., de Wet, C., Montañez, I., et al. (2021). A mechanistic understanding of oxygen isotopic changes in the Western United States at the Last Glacial Maximum. *Quaternary Science Reviews*, *274*, 107255. https://doi.org/10.1016/j.quascirev.2021.107255

Thompson, R. S., & Anderson, K. H. (2000). Biomes of western North America at 18,000, 6000 and 0 ^{14}C yr BP reconstructed from pollen and packrat midden data. *Journal of Biogeography*, *27*(3), 555–584. https://doi.org/10.1046/j.1365-2699.2000.00427.x

Trachsel, M., & Telford, R. J. (2017). All age–depth models are wrong, but are getting better. *The Holocene*, *27*(6), 860–869. https://doi.org/10.1177/0959683616675939

Wendt, K. A., Dublyansky, Y. V., Moseley, G. E., Edwards, R. L., Cheng, H., & Spotl, C. (2018). Moisture availability in the southwest United States over the last three glacial-interglacial cycles. *Science Advances*, *4*(10), eaau1375. https://doi.org/10.1126/sciadv.aau1375

Woolfenden, W. B. (2003). A 180,000-year pollen record from Owens Lake, CA: Terrestrial vegetation change on orbital scales. *Quaternary Research*, *59*(3), 430–444. https://doi.org/10.1016/s0033-5894(03)00033-4

References From the Supporting Information

Christen, J. A., & Pérez, S. (2009). A new robust statistical model for radiocarbon data. *Radiocarbon*, *51*(3), 1047–1059. https://doi.org/10.1017/s003382220003410x